ELSEVIER

Ultrasound in Med. & Biol., Vol. 22, No. 8, pp. 959–977, 1996

0301-5629/96 $15.00 + .00

PII: S0301-5629(96)00120-2

●*Review*

IMAGING OF THE ELASTIC PROPERTIES OF TISSUE—A REVIEW

L. GAO,[†] K. J. PARKER,[†‡] R. M. LERNER* and S. F. LEVINSON[†§]

[†]Department of Electrical Engineering and Center for Biomedical Ultrasound, University of Rochester, Rochester, NY; [‡]Department of Radiology, Strong Memorial Hospital, Rochester, NY; *Department of Diagnostic Radiology, Rochester General Hospital, Rochester, NY; and [§]Department of Orthopedics, Division of Rehabilitation Medicine, Strong Memorial Hospital, Rochester, NY

(*Received* 5 *May* 1995; *in final form* 8 *May* 1996)

Abstract—Recently, a number of methods have been developed that make it possible to image the elastic properties of soft tissues. Because certain types of tissues such as malignant lesions, for example, have elastic properties that are markedly different from surrounding tissues, elasticity imaging could provide a significant adjunct to current diagnostic ultrasonic methods. Further, elasticity imaging techniques could be used to augment the study of tissues that change their elastic properties, such as skeletal and cardiac muscle. In this paper, we survey some of the previous work done in the related field of biomechanics, and we review measurement techniques from the 1950s to the 1980s. Different approaches to elastic imaging and signal processing are then discussed and a lexicography for elastic imaging is introduced. It is hoped that this nomenclature will provide a meaningful categorization of various approaches and will make evident the inherent parameters displayed and conditions applied in deriving the resulting images. Key assumptions and signal processing approaches are also reviewed. Finally, directions for future work are suggested.

Key Words: **Elastography, Sonoelasticity, Shear, Vibration, Hardness, Elastic modulus, Shear modulus, Tumor detection, Tissue motion.**

INTRODUCTION

Imaging of the elastic properties of tissues has become the subject of increasing research effort. The goal of elastic imaging is to map tissue properties such as Young's modulus (or stiffness), Poisson's ratio and viscosity in an anatomically meaningful presentation to provide useful clinical information. Perhaps the most important parameter among them is Young's modulus, because of its dependence upon the composition of the tissue. Changes in soft tissue stiffness may be related to an abnormal pathological process; for example, some tumors of the breast, liver and prostate are detected by palpation through the overlying tissue. Physicians have relied on palpation of hard areas in tissue to aid in tumor detection. Present cross-sectional imaging methods display tissue parameters not directly associated with the findings on palpation.

We now propose to use the term "elastography" for the general field of elasticity imaging; the images thus acquired are elastograms. This field may be considered a merger of several related fields, which have long and distinguished histories:

1. The study of tissue elastic constants (biomechanics);
2. The study of tissue contrast differences and tissue motion by using imaging systems (X-ray, ultrasound, MRI, stroboscopes and others) (radiology);
3. The study of vibrating targets by using coherent radiation (laser, sonar and ultrasound) (biology, physics and nondestructive testing).

The fundamental techniques in these fields will be referred to as prior studies. They will be covered briefly in the first part of this review. Then, elastography techniques developed by current research groups will be presented in more detail. We focus our review on published papers in the archival literature.

PRIOR STUDIES

The study of tissue elastic constants (biomechanics)

A comprehensive review of this field is out of the scope of this paper; however, some basic concepts and

Address correspondence to: Kevin J. Parker, Department of Electrical Engineering, University of Rochester, Rochester, NY 14627, USA.

works directly related to elastic imaging are considered. The stress–strain relationship for most tissues is nonlinear. Also, a hysteresis loop is encountered in cyclic loading and unloading, and stress tends to relax over time under constant strain. Many models have been proposed relating stress and strain based on the linear theory of viscoelasticity, as described by Voigt, Maxwell and Kelvin. Buchthal and Kaiser (1951) proposed a model with a continuous relaxation spectrum that corresponds to a combination of an infinite number of Voigt and Maxwell elements. Viidik (1966) constructed a nonlinear theory of the Kelvin type. Fung (1981) formulated a quasilinear viscoelasticity theory of soft tissue. His argument was that for oscillations of small amplitude around the equilibrium state, the theory of linear viscoelasticity should apply, while for finite deformation, his theory accounts for the nonlinear stress–strain characteristics. Figure 1 summarizes the principal features of viscoelastic models. Note that Fig. 1, from biomechanics, is analogous to the theory of multiple relaxation frequencies, which has been used for many years in ultrasound as an explanation for the linear frequency dependence of attenuation (Carstensen and Schwan 1959; Pauly and Schwan 1971). It must be kept in mind, however, that for each case, biomechanics and ultrasonics, the applicable frequencies and the details of the relaxation mechanics are quite distinct.

Truong (1971) measured the velocity and attenuation coefficient of longitudinal waves propagated along thin muscles and showed the dependence of these constants on frequency. Taber (1984) studied the elastic behavior of the pig eyeball under rigid cylindrical indentures and observed the highly nonlinear stress–strain relations. Levinson (1987) studied the speed of ultrasound wave propagation in frog sartorius specimens and proposed a linear transverse anisotropic model. Parker et al. (1993) measured the linear and nonlinear Young's modulus of canine and human prostate specimens. Although there are well-established models for measurements of elastic tissue parameters, few tissue types have been reported and there are broad gaps in our knowledge of the elastic properties of normal and diseased tissues. There is little information on the elastic properties of different components of structured organs (those containing separate regions of distinct tissue types) such as the kidney, breast and prostate. The reaction of normal parenchyma to different tumors and lesions is also an area of unresolved speculation. Thus, there remains a need for basic measurements and characterization of tissue types, to provide a foundation for modeling and for interpretation of elastograms.

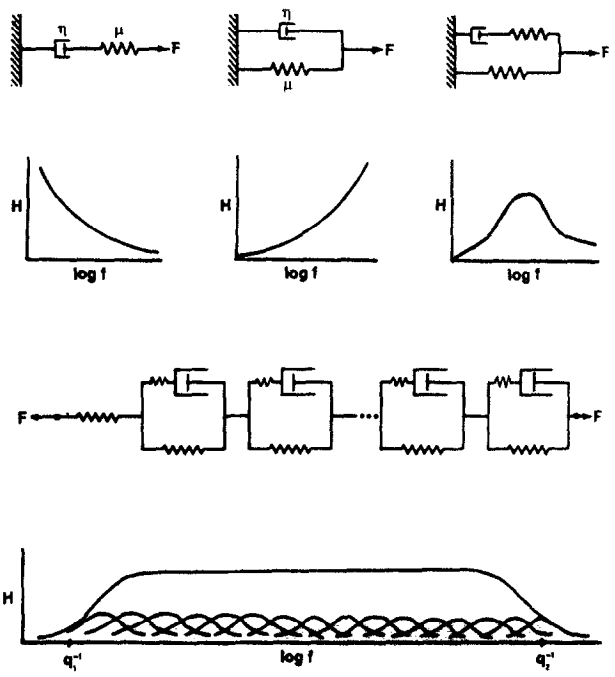

Fig. 1. A summary of the principal features of viscoelastic models. Three standard viscoelastic models, namely, the Maxwell, Volgt and Kelvin models are shown in the top row, and a mathematical model of the viscoelasticity of biological soft tissues is shown in the third row. Figures in the second row show the relationships between the hysteresis (H) and the logarithm of frequency (ln f) of the three models immediately above. The figure in the bottom row shows the general hystersis-log frequency relationship of most living soft tissues, corresponding to the model shown in the third row. For the soft tissue model the springs are nonlinear, and each Kelvin unit contributes a small bell-shaped curve, the sum of which is flat over a wide range of frequencies. (Reprinted with permission from: Fung YC. *Biomechanics: Mechanical properties of living tissues.* New York, NY: Springer-Verlag, Inc., 1981, p. 288, Fig. 7.6:5. ISBN 0-387-97947-6.)

The study of tissue motion using an imaging system

Oestreicher and colleagues (Oestreicher 1951; Von Gierke et al. 1952) studied the behavior of the human body surface subjected to sound fields or mechanical vibration. They used a strobe light and photography to acquire surface wave propagation patterns, thus obtaining the wavelength and wave speed. They also formulated a theory to explain the increase of impedance of tissue with increased frequency. The shear modulus could be calculated from their experimental data.

Wilson and Robinson (1982) presented a signal processing technique to measure small displacements of liver tissue caused by aortic pulsation and vessel diameter variations. They obtained radio frequency (RF) M-mode signals, and on the assumption that the tissue follows points

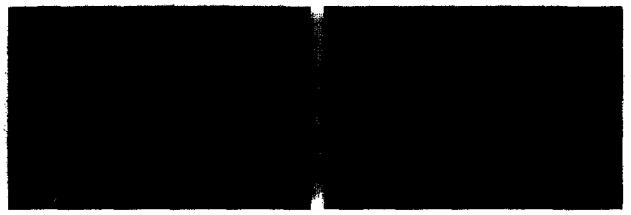

Fig. 2. Curves of tissue displacement and compression. (Reprinted with permission from: Wilson LS, Robinson DE. Ultrasonic measurement of small displacements and deformations of tissue. *Ultrasonic Imaging* 1992;4:71–82, Figure 5a.)

of constant phase, they calculated the velocity of tissue motion from the trajectory of a constant phase point. The integral of velocity over time gave a rough estimate of displacement (refer to Fig. 2).

Dickinson and Hill (1982) used the correlation coefficient between successive A-scans to measure the amplitude and frequency of tissue motion. They set up a correlation parameter to measure the changes of the interrogated region between two successive A-scans. The correlation parameter is unity for stationary tissue and decreases monotonically with increased tissue motion. Their assumption is that the decorrelation is proportional to displacement, which is only true for very small displacement. This technique was further developed by Tristam et al. (1986, 1988) to look at the different responses of normal liver and cancerous liver to cardiac movement. They found some features on the correlation curves to distinguish normal liver from that with tumor. Those features included: livers with tumor generally have lower maximum values, fewer peaks, and greater regularity (refer to Fig. 3). De Jong et al. (1990) used a modified correlation technique to measure tissue motion, where they found the maximum cross-correlation by an interpolation algorithm. The peak location of the cross-correlation function may also be determined by several other methods, such as: oversampling, sinc-interpolation and fitting other curves like parabolas to the neighborhood of the peak of the cross-correlation function. The method of De Jong et al. (1990) is limited to narrow-band signals, where the cosine function still represents a good approximation.

Fetal lung elasticity may be an important indicator of pulmonary maturity and has been used to determine if the lungs are developing normally. Birnholz and Farrell (1985) tried to qualitatively determine the stiffness of fetal lung by evaluating ultrasound B-scans, where one can see the compression of lung due to cardiac pulsations. They argued that stiff lung tissue transmits cardiac pulsations moving as a block without regional deformation, whereas soft lung tissue compresses, with maximal deformation immediately adjacent to the heart. Adler et al. (1989, 1990) arrived at more quantitative estimates. They applied correlation techniques to digitized M-mode images and estimated <r>, a parameter that characterizes the range of transmitted cardiac motion in fetal lung. The parameter is actually the temporally and spatially averaged systolic to diastolic deformation per unit epicardial displacement (Fig. 4).

Eisensher et al. (1983) applied a 1.5-Hz vibration source to liver and breast tissue and used M-mode ultrasound to look at the induced quasistatic compression. They found that the quasistatic compression response from benign lesions was characteristically sinusoidal, whereas those from malignant tumors tended to be more flat, *i.e.*, more of a nonlinear response.

Krouskop et al. (1987) reported one of the first quantitative measurements of tissue elasticity using gated pulsed Doppler. The set of equations relating tissue properties and tissue movements reduces to some very simple forms under the assumption of isotropy and incompressibility, and the final problem of finding tissue elasticity reduces to measuring tissue peak displacements and their gradients. A single A-line pulsed Doppler instrument was used in their experiments to measure actual tissue flow at points of interest under external vibration. They suggested a possible measurement of tissue stiffness in a very small region, *i.e.*, 0.5 × 0.5 mm.

The study of vibrating targets using coherent radiation

Laser, sonar and ultrasound have been used to extract the motion parameters of a vibrating target.

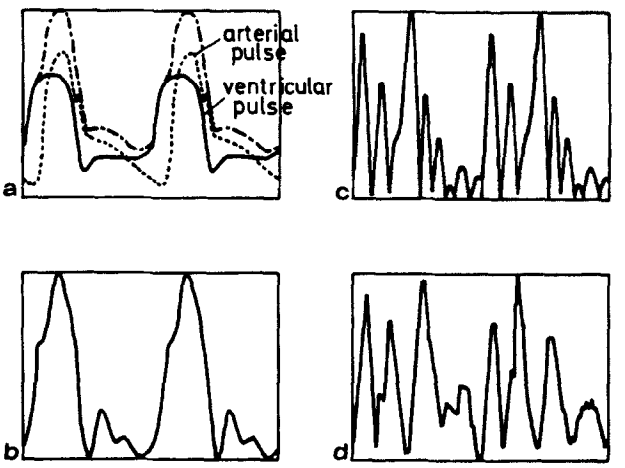

Fig. 3. Comparison of simulated and measured correlation patterns: (a) pressure profile, (b) displacement, (c) simulated correlation pattern, (d) measured correlation pattern (horizontal axis: time of two oscillations). (Reprinted with permission from: Tristam M, et al. Application of Fourier analysis to clinical study of patterns of tissue movement. *Ultrasound in Medicine & Biology* 1988;14(8):705, Figure 8.)

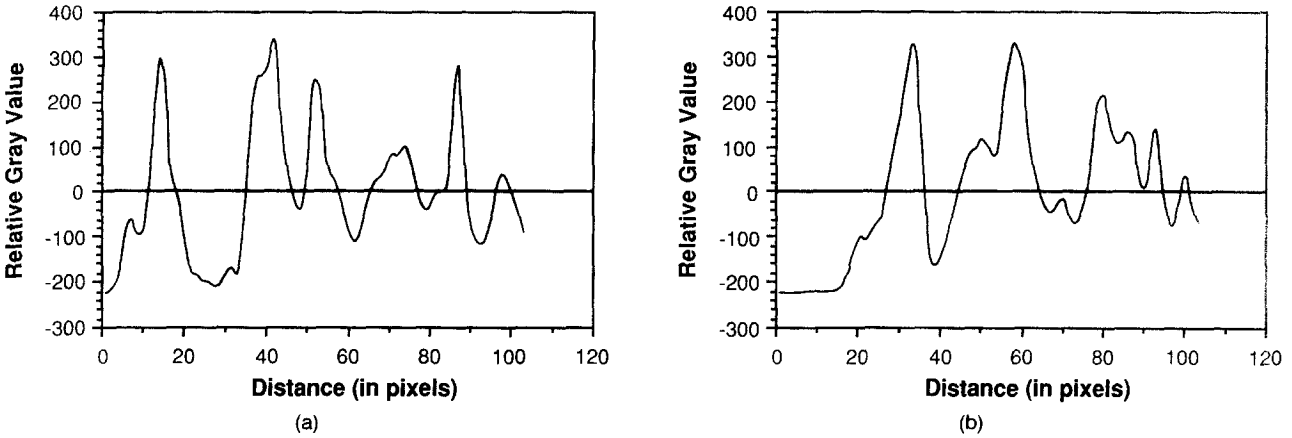

Fig. 4. Example of the time-averaged relative gray-scale distribution from (a) systolic and (b) diastolic lines of data. Multiple peaks corresponding to bright reflectors in the M-mode image are distributed relatively uniformly throughout the fetal lung. Approximate distance conversion in this example is 0.22 mm/pixel. The epicardial reflector results in the peak closest to the origin, which subsequently undergoes the maximum shift in going from systole to diastole relative to the remaining gray-scale peaks. (Reprinted with permission from: Adler RS, et al. Quantitative tissue motion analysis of digitized M-mode images: Gestational differences of fetal lunch. *Ultrasound in Medicine & Biology* 1990;16(6):566, Figure 5.).

Applications include military targets and nondestructive testing of devices. The typical parameters of interest are displacement amplitude, phase and frequency. Conventional medical Doppler ultrasound is designed to characterize steady and slowly varying blood flow and is not suitable for detection of a vibrating target. Most of the early techniques for blood flow measurement used frequency domain Doppler spectral analysis to characterize the velocity profile as a function of the cardiac cycle. Detection of the displacement and frequency of a vibrating target (with no steady or net displacement) requires a very different detection algorithm (Huang et al. 1990, 1992).

The Doppler spectrum of the scattered ultrasound signal from a vibrating target is similar to that of a pure-tone frequency modulation process under certain conditions. It has symmetric side harmonics around the carrier frequency. The spacing of the harmonics is equal to the target vibrating frequency, and the amplitudes of the harmonics are given by successive Bessel functions of the first kind. The expression for the signal is (Taylor 1976):

$$s_r(t) = A \sum_{-\infty}^{\infty} J_n(\beta)\cos[\omega_0 t + n(\omega_L t + \varphi)] \quad (1)$$

The modulation parameter β of the Bessel function is proportional to the target vibrating amplitude. ω_0 is the angular frequency of the ultrasound signal, ω_L is the angular frequency of the target vibration and ϕ is the vibration phase.

Taylor (1976, 1981) used a laser Doppler technique to measure the vibrating velocity of suspended particles and to calibrate microphones. He measured the relative magnitude of the Bessel band and found the vibration amplitude by fitting the data to the theoretical spectrum.

Holen et al. (1985) observed this characteristic Bessel-band Doppler spectrum when using Doppler ultrasound to examine unusually oscillating heart valves. The Doppler spectrum changes dramatically when the product of the Fast Fourier Transform time and the frequency of the vibrating target varies from less than unity to larger than unity. When the product was larger than unity, the vibration frequency of oscillating heart valves was determined by the spacing between harmonics in the Doppler spectrum. The vibration amplitude was estimated by counting the number of significant harmonics, as an approximation to the frequency modulated bandwidth, which is proportional to the amplitude of the vibrations (Fig. 5).

Cox and Rogers (1987) studied the Doppler ultrasound response of fish auditory organs to a low-frequency sound field. The vibration amplitude of the hearing organ was determined by comparing the ratio of the carrier and the first side band of the Doppler spectrum. Jarzynski et al. (1988) performed a similar study using scattered laser Doppler from vibrating particles in water.

The techniques described above can be classified as a ratio method, because they are all related to some amplitude ratios of the harmonics. Huang et al. (1990)

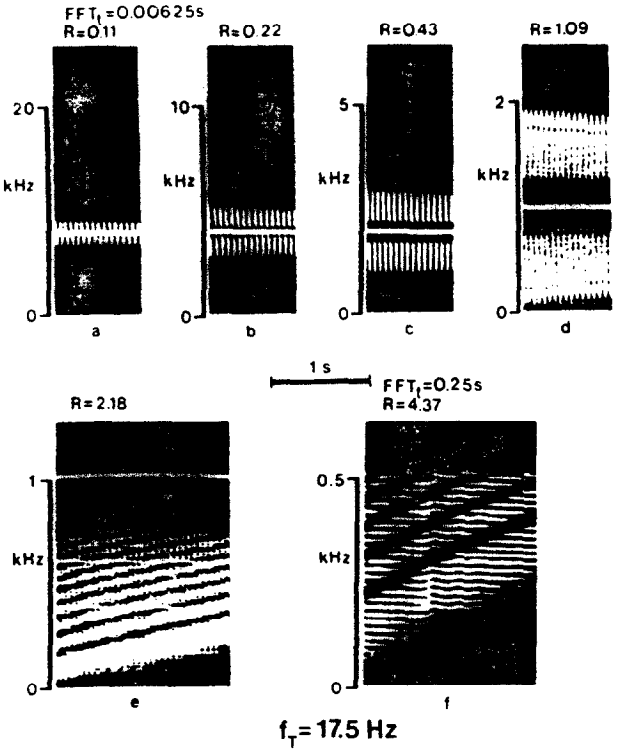

Fig. 5. Doppler registrations of 17.5 target that demonstrate the effects of the duration of FFTt. In (a) – (f) the character of the display changes as the value of FFTt increase. In (a), R << 1 and the Dopler frequencies are clustered about a sinusoid with frequency 17.5 Hz, whereas in (f), R >> 1 and the Doppler frequencies are arranged in horizontal lines spaced 17.5 Hz apart. It is a feature of the frequency analyzer used that the displayed frequency range decreases as FFTt is increased. Thus, in (e) and (f) only frequencies smaller than the baseline frequency are shown: in (f) the baseline frequency is larger than the display range and is, therefore, not present on the display. The absence of frequencies in a zone adjacent to the baseline is due to high pass filtration in the Doppler instrument. (Reprinted with permission from: Holen J, et al. Representations of rapidly oscillating structure on the Doppler display. *Ultrasound in Medicine & Biology* 1985;11(2):269, Figure 2.)

developed an estimator measuring the spectral spread (or variance) of the Doppler spectrum, which was applied for vibration amplitude sonoelastography.

ELASTOGRAPHY TECHNIQUES

For centuries, physicians have used palpation to detect abnormal regions of increased Young's modulus (hardness or stiffness) as an indicator of cancer. The concept of elastography was developed as a qualitative and quantitative technique to map tissue elasticity, thus potentially adding new, clinically useful information to the interpretation of ultrasound, CT or other scans.

Various elastography techniques have been developed using different modalities (ultrasound, MRI and optics), employing different tissue excitations and extracting different parameters of tissue motion. To better understand their distinctions, we now propose the following nomenclature:

1. Elastography: the general field of elasticity imaging;
2. Sonoelastography: the use of ultrasound for imaging of tissue elastic parameters.

Either of the above terms could be modified by terms that describe the method of tissue deformation and the parameters that are imaged:

1. Strain: images displaying tissue strain;
2. Stress: images displaying tissue stress;
3. Velocity: images displaying velocity of tissue motion;
4. Amplitude: images displaying amplitude of tissue motion;
5. Phase: images displaying phase of tissue motion;
6. Vibration: images based on propagation of vibrations through tissue;
7. Compression: images based on static or nearly static compression of tissue;
8. Quasistatic: images based on very low frequency (less than 10 Hz) vibrations;
9. Functional: images utilizing derivative, integral or functional quantities.

Other modifiers could be added as needed.

Vibration amplitude sonoelastography

Lerner and Parker presented preliminary work on vibration amplitude sonoelastography (sonoelasticity imaging) in 1987 (Lerner and Parker 1987). In vibration amplitude sonoelastography, a low-frequency vibration (20–1000 Hz) is externally applied to excite internal vibrations within tissue under inspection. A stiff inhomogeneity inside surrounding soft tissue produces a disturbance in the normal vibration eigenmode patterns. Doppler detection algorithms are employed to make a real-time vibration image. In some organs, modal patterns can be created, revealing additional information as to the shear wave speed of sound in the tissue (Parker and Lerner 1992).

The first vibration amplitude sonoelastography image, published by Lerner and Parker (1987) and again by Lerner et al. (1988), is reproduced in Fig. 6. This crude image shows the vibration within a sponge containing a hard region (lower dark region). The sponge was vibrated from below, and pulsed, range-gated Doppler was used to determine the vibration amplitude within its interior. By 1990, the University of Rochester group was using a modified color Doppler

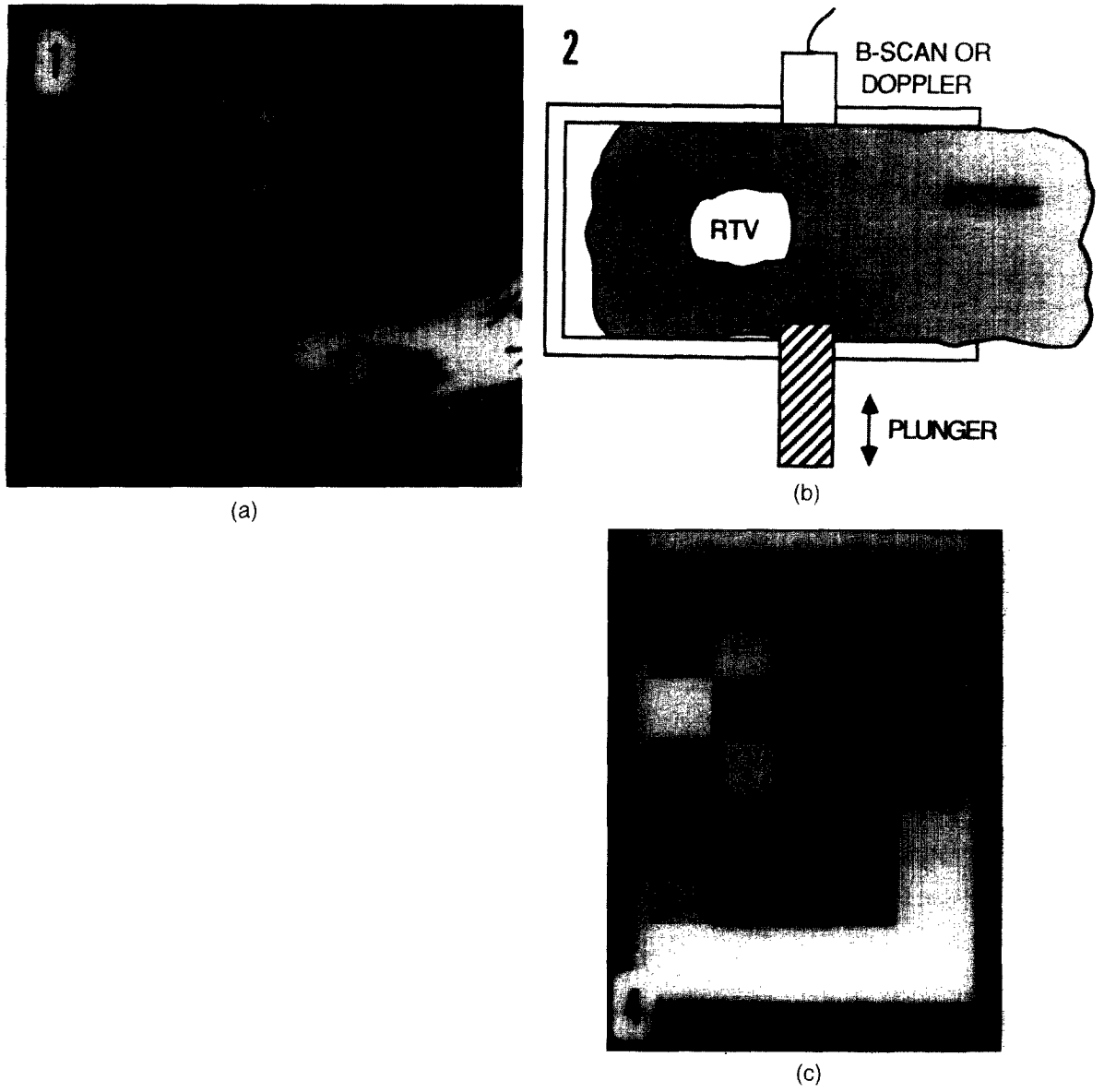

Fig. 6.(a) A 2.5 MHz B-scan image of sponge phantom with stiff, RTV tumor embedded (arrow-heads). The higher attenuation within the RTV results in some shadowing (lower left). (b) Schemetic illustration of inhomogeneous sample with mechanical vibration and B-scan imaging or Doppler range gate measurement. (c) Computer generated image of sponge RTV phantom using range-gated Doppler peak velocities measured as a function of position. The geometry corresponds to Figs. 6(a) and 6(b). Resolution is 7 blocks vertical (5 mm each) by 5 blocks horizontal (roughly 1 cm transverse each), thus the aspect ratio is different from Figs. 6(a) and 6(b). Gray scale brightness corresponds to measured peak velocities within the sample volume, varying linearly from white (2.5 KHz Doppler shift) to black (< 300 Hz Doppler shift). The bottom row is white due to the measurement of plunger vibration. The tumor region appears dark because of low peak velocities not because of its lower backscatter. This is explained by the preferential movement of the surrounding, more compliant sponge. (Reprinted with permission from: Lerner RM, et al. Sono-elasticity: Medical elasticity images derived from ultrasound signal in mechanically vibrated targets. *Acoustical Imaging* 1988;16:317–327, Figs. 1, 2 and 4.)

instrument to make real-time vibration amplitude sonoelastography images, albeit bistable images, where vibration above a threshold produced a saturated red. Reports in 1990 described measurements of tissue elastic constants, finite element models for vibration amplitude sonoelastography and results of phantom and *ex vivo* phantom studies (Lerner et al. 1990; Parker et al. 1990). By 1992, studies of liver, breast and kidney

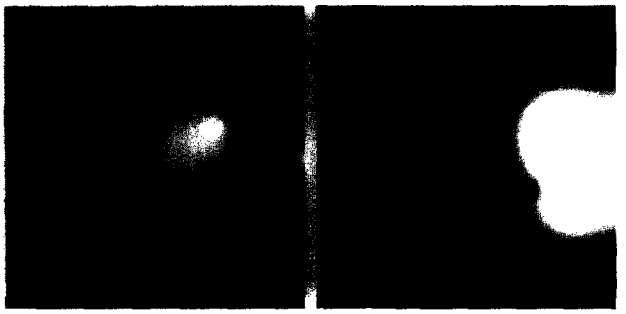

Fig. 7. Theoretical prediction of 60 Hz vibration on right-hand side of two elastic media, (a) soft lesion, (b) hard lesion.

were published, and a study of *ex vivo* prostate cancer detection was completed (Lee et al. 1991; Parker and Lerner 1992). In 1994, a real-time *in vitro* study of prostate had been completed, demonstrating that vibration amplitude sonoelastography had better sensitivity and predictive value than did B-scan imaging alone (Rubens et al. 1995). Furthermore, in 1994 a mathematical model for vibration amplitude sonoelastography was completed (Gao et al. 1995). A sonoelastic Born approximation was used to solve the wave equations in an inhomogeneous (but isotropic) medium. The total wave field inside the medium can be expressed as:

$$\Phi_{\text{total}} = \Phi_i + \Phi_s \tag{2}$$

where Φ_i is the homogeneous field or incident field, and Φ_s is the field scattered by the inhomogeneity. They satisfy, respectively:

$$(\nabla^2 + k)\Phi_i = 0 \tag{3}$$

$$(\nabla^2 + k)\Phi_s = \alpha(x) \tag{4}$$

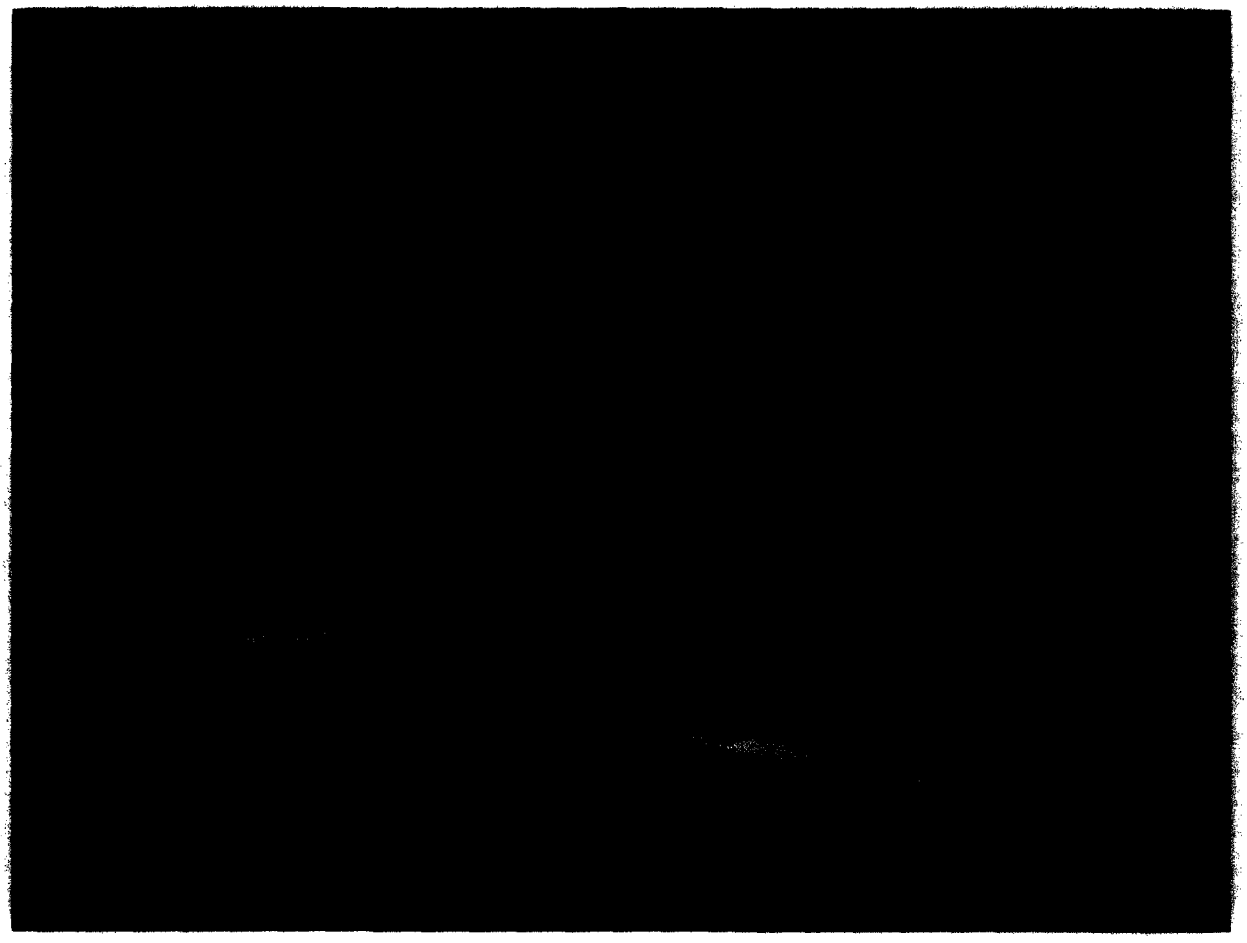

Fig. 8. Sonoelasticity of the whole prostate. Vibration is applied near the pelvic bone, and green indicates conduction of vibration. A biopsy-confirmed tumor T is outlined by the vibration pattern.

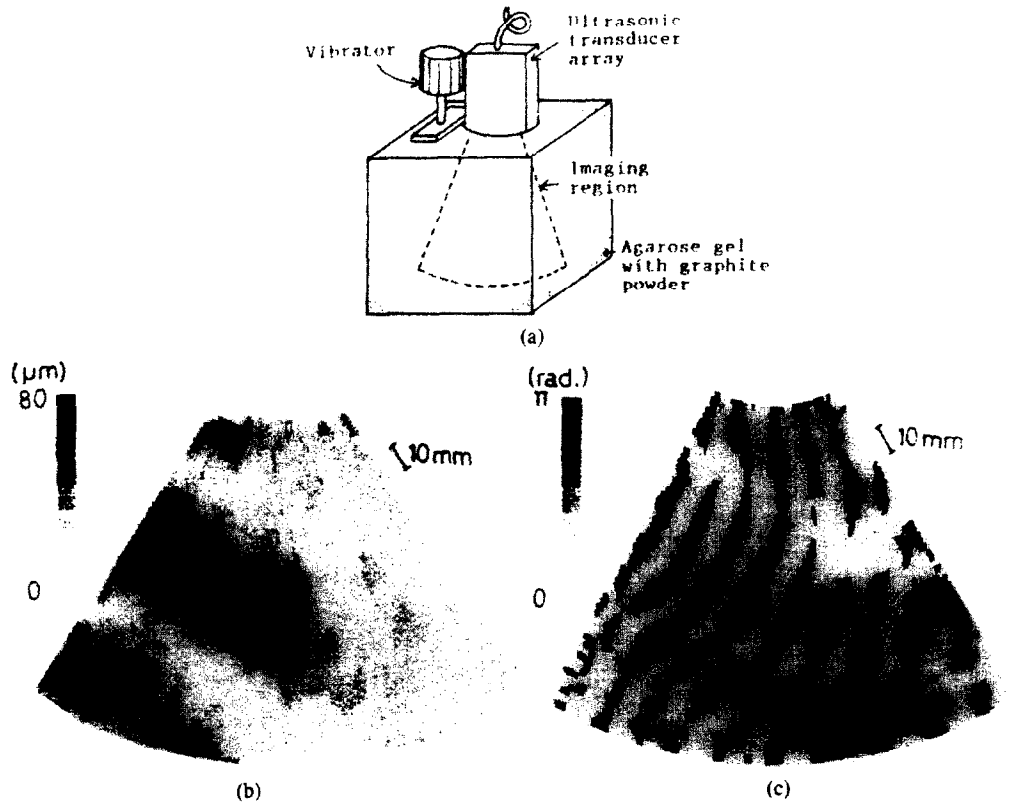

Fig. 9. Phase maps for uniform agarose gel phantom. (a) Vibrator is placed at left side of ultrasonic transducer array. (b) Amplitude map. (c) Phase map. Frequency of vibration is 200 Hz. (Reprinted with permission from: Yamakoshi Y, et al. Ultrasonic imaging of internal vibration of soft tissue under forced vibration. *IEEE Transactions on Ultrasonics, Ferroelectrics, and Frequency Control* 1990;37(2):45–53, Figure 7. ©1990 IEEE.)

where $\alpha(x)$ is a function of the properties of the inhomogeneity. Figure 7 shows the situation where a hard and a soft lesion appear as disturbances in a regular vibration pattern. In the image on the right-hand side, a hard lesion shows lower vibration amplitude than the surrounding medium, and the medium is under 60-Hz vibration excitation. For the image on the left-hand side, a soft lesion shows higher vibration amplitude than the surrounding medium, and the vibration frequency is 100 Hz. Figure 8 shows an example of *in vitro* real time-prostate detection using vibration amplitude sonoelastography. The region marked with T was later determined by pathology to be a hard tumor, and it appeared as void of vibration on the sonoelastogram. (The green scale brightness is proportional to vibration amplitude.)

Another aspect of vibration amplitude sonoelastography to be considered is the signal processing issue. Huang et al. (1990) proposed a technique to estimate β (refer to eqn 1) from the spectral spread. The simple relationship between β (which is proportional to the vibration amplitude of the target) and the spectral spread σ_ω they found is:

$$\beta = \sqrt{2}(\sigma_\omega/\omega_L). \quad (5)$$

where ω_L is the vibration frequency of the vibrating target. This is a simple but useful special property of the Bessel Doppler function. They also investigated the effect of noise, sampling and nonlinearity on the estimation. A later paper by Huang et al. (1992) extended this work to real-time estimators of vibration amplitude, phase and frequency that could be used for a variety of vibration sonoelastography techniques.

Vibration amplitude sonoelastography detects a hard lesion by looking at the disturbance in the amplitude of the vibration pattern. An interesting observation is that one can produce a vibration modal pattern in some organs, and these patterns have quantitative tissue characterization applications. In practice, the lowest frequency modes are preferred, as they are the easiest to excite and the easiest to interpret. Various

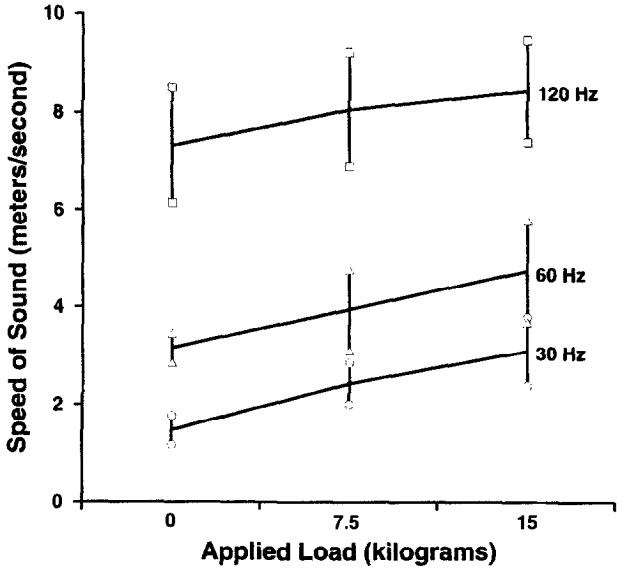

Fig. 10. Measured values of speed of sound, *in vivo*, under different frequencies and loading conditions, for human muscle.

time and frequency estimators make this technique a real-time diagnostic tool. Vibration amplitude sonoelastography is currently in an early stage of *in vivo* trials using real-time imaging techniques.

Vibration phase gradient sonoelastography

Sato et al. (1985) were involved with the study of nonlinear interactions between ultrasound and lower frequency waves in tissue and at the time that Parker and Lerner, and Krouskop and Levinson, were using linear methods to investigate the propagation of vibrations inside tissue. In the late 1980s, Sato (Yamakoshi et al. 1990) developed a vibration phase gradient approach to sonoelastography that built on his earlier work and on the work of other investigators. His technique maps both the amplitude and the phase of low-frequency wave propagation inside tissue, and from these maps, the wave propagation velocity and dispersion properties are derived. These parameters are directly linked to the elastic and viscous characteristics of tissue.

Because the phase modulated (PM) Doppler spectrum of the signal returned from sinusoidally oscillating objects is similar to that of a pure-tone frequency modulation (FM) process, the tissue vibration amplitude and phase of tissue motion may be estimated from the ratios of adjacent harmonics.

From eqn (1), the amplitude ratio between adjacent Bessel bands of the spectral of the signal is:

$$A_{i+1}/A_i = |J_{i+1}(\beta)/J_i(\beta)|. \quad (6)$$

If A_{i+1}/A_i is calculated as a function of β beforehand, then β can be estimated from the experimental data.

Phase and amplitude maps (Fig. 9) constructed as a function of time permit the display of wave propagation as a moving image. Images of amplitude and phase are computed offline by using a minimum squared error algorithm to estimate the direction of wave propagation and to calculate phase and amplitude gradients in this direction. Preliminary *in vivo* results have been demonstrated (Yamakoshi et al. 1990) under the assumption that the effect of shear viscosity is negligible at low frequencies.

Levinson (1995) adapted and refined Sato's technique (Yamakoshi et al. 1990) by using a more general model of tissue viscoelasticity and by using a linear recursive filtering algorithm based on cubic B-spline functions. By taking the Fourier transform of the wave equation, he found that the frequency domain displacement equation for a linear, homogeneous, isotropic viscoelastic material can be written as:

$$-\rho\omega^2\mathbf{U} = (\mu + i\omega\eta) \times \nabla^2\mathbf{U} + [(\mu + \lambda) + i\omega(\eta + \kappa)]\nabla\nabla\cdot\mathbf{U} \quad (7)$$

where $\mathbf{U}$ is the temporal Fourier transform of the internal tissue displacement, ρ is the density, μ and λ are the shear and longitudinal moduli of elasticity (also known as the Lamé constants) and η and κ are the shear and longitudinal coefficients of viscosity, respectively. This equation can lead to expressions that relate the shear modulus of elasticity and viscosity to the wave number and the attenuation coefficient of the wave. It has also been suggested that these moduli could be calculated directly from eqn (7), although methods of estimating the Laplacian in three dimensions do not currently exist.

Using the assumptions that viscosity at low frequencies is negligible and that shear waves predominate, Levinson et al. (1995) conducted a series of experiments on the quadriceps muscle group in human thighs. Values of Young's modulus of elasticity were calculated from phase gradient images of the subjects' thighs under conditions of active muscle contraction. A pulley apparatus was used to control the tension applied to the muscle. As expected, the measured speed of vibration propagation and the calculated values of Young's modulus increased with increasing degrees of contraction as needed to counteract the applied load. Their speed-of-sound data are shown in Fig. 10.

Compression strain sonoelastography

Ophir and colleagues (Ophir et al. 1991) have developed an imaging technique (elastography as they

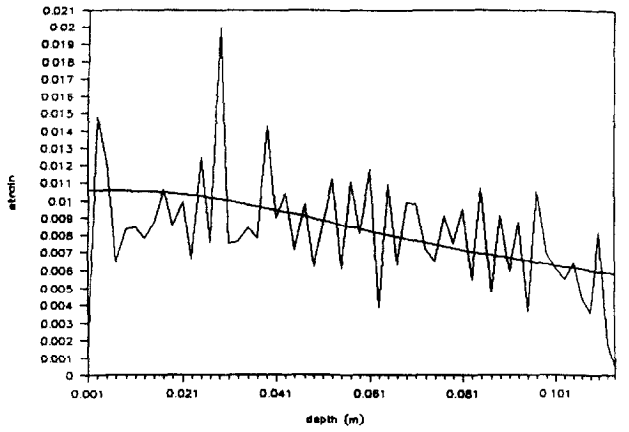

(a)

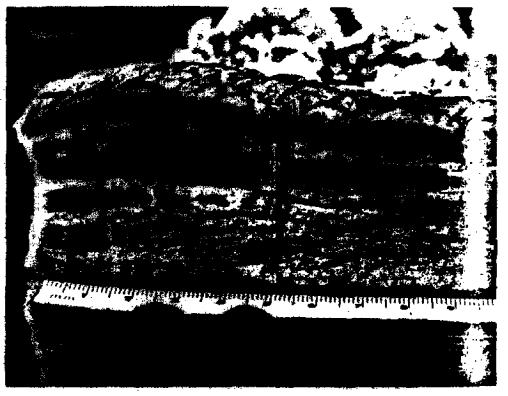

(b)

Fig. 11. Bacon slab and its images. (a) Raw data—strain vs. depth; (b) photograph of cut section (only the region between the 10 and 50 mm marks was scanned).

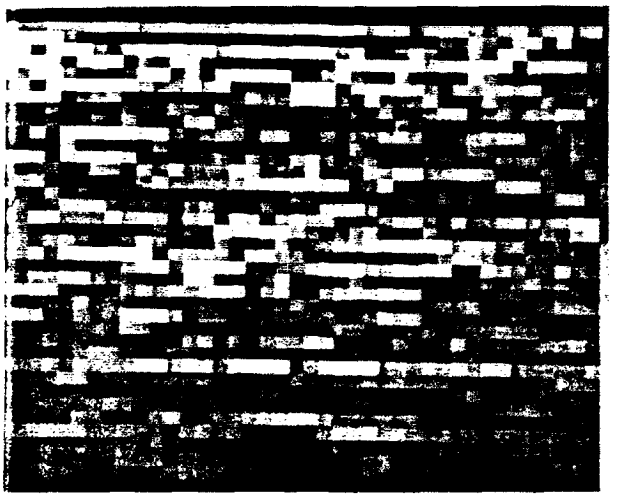

(c)

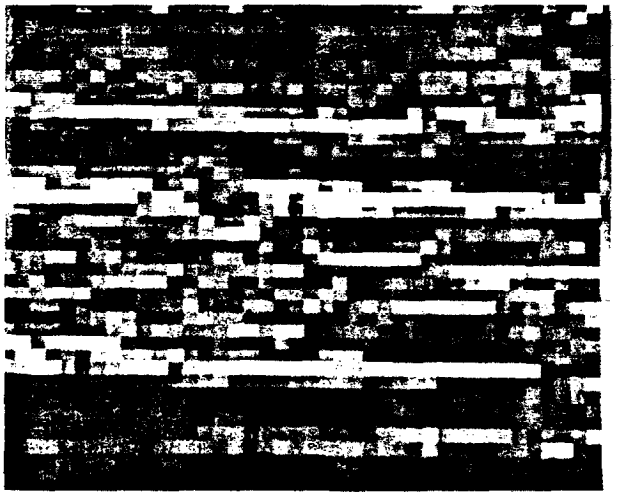

(d)

Fig. 11. *Continued.* (c) B-scan; (d) strain image. Note clear definition of certain tissue strata. (Reprinted with permission from: Ophir J, et al. Elastography: A quantitative method for imaging the elasticity of biological tissues. *Ultrasonic Imaging* 1991;13:126, Figure 8.)

named it) that is based on the static deformation of a linear, isotropic, elastic material. They externally compressed the tissue under inspection and used cross-correlation analysis on the pre- and postcompression A-line pairs. From these data, they were able to calculate the strain profile inside the tissue along the transducer axis. They measured the stress field close to the transducer surface and added corrections for the nonuniform stress field inside tissue. Having both strain and stress fields, they calculated the elastic modulus profile of the tissue and displayed the information as an elastogram.

The first RF A-line is obtained with the transducer slightly precompressing the target to ensure good contact; the second A-line is obtained after axially compressing the target an additional increment dz (usually dz is about 1% of the target length). The echoes are broken into small overlapping segments (4-mm segments overlapping 1 or 2 mm in Ophir et al. (1991)). The postcompression A-line is 2dz/c shorter than the precompression A-line, where c is the speed of the ultrasound in the target. The postcompression A-line is zero-padded to have the same length as the precompression one. Cross correlation is applied between congruent segments in an A-line pair. The temporal location of the maximum peak of the cross-correlation function is the estimate of the time shift between the two segments. The time scale is relative to the face of the transducer, so the shift of the signal starts as zero at the beginning of the A-line and increases to 2dz/c at the end. If the elastic modulus differs somewhere along the line, little or no increase will show in the time shift of certain segments. After one A-line pair is processed, the corresponding strain profile is defined

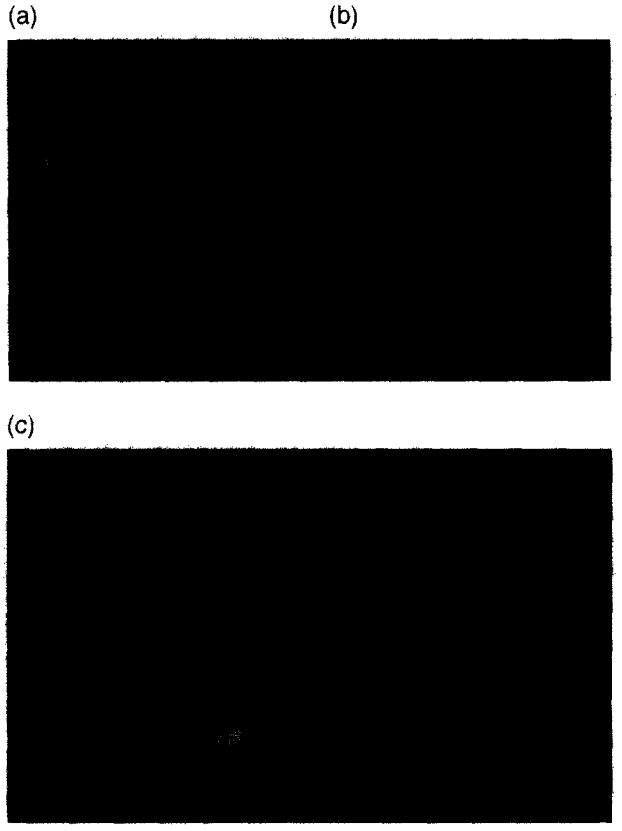

Fig. 12. Elastogram (b) and sonogram (a) of a transverse cranio-caudal section of the right breast of a 62-year-old. The corresponding radiograph (c) is also shown. (Reprinted with permission from: Céspedes I, et al. Elastography: Elasticity imaging using ultrasound with application to muscle and breast in vivo. *Ultrasonic Imaging* 1993;15:84, Figure 7.)

as a one-dimensional graph showing the strain as a function of depth in the target. The quantity shown in eqn 8 is a particular local estimate of the strain in the ith depth increment:

$$s_i = \frac{t_{i+1} - t_i}{2dz/c} \qquad (8)$$

Where t_i is the time shift for segment i. After repeating the process for an array of all A-lines, a strain image of the compressed target is obtained (Fig. 11).

For stress distribution, Ophir et al. (1991) used the uniform model at the beginning. Later, these workers (Ponnekanti et al. 1992) developed a more realistic model based on Saada's (1974) theory. This model accounts for the stress behavior of decaying away from the compressor, and increasing again when close to the base of the target. As the range of strain measurement starts from zero up, they choose to display the inverse of elastic modulus in the elastogram (the image displaying stiffness), so that it has a finite range. Some phantom *in vitro* and *in vivo* experiments showed some elastic structures that do not appear on the conventional B-scan images (Céspedes et al. 1993; refer to Fig. 12). This technique may be used to detect tumors with increased stiffness inside compressible soft tissue.

There are some signal processing issues and artifacts associated with the cross-correlation method mentioned above. The estimation of the time shift tends to favor regions with large envelope amplitude within the estimation window. Céspedes and Ophir (1993) proposed some pre-cross-correlation amplitude compression technique to reduce the artifacts, and they also proposed a signal stretching method. Cross-correlation is used to analyze A-line pairs to obtain strain information in this technique. Some approximate stress distribution inside tissue has to be assumed for final elasticity reconstruction. The basic model is two-dimensional. Data processing is done offline. Some preliminary *in vivo* results are shown in Céspedes et al. (1993).

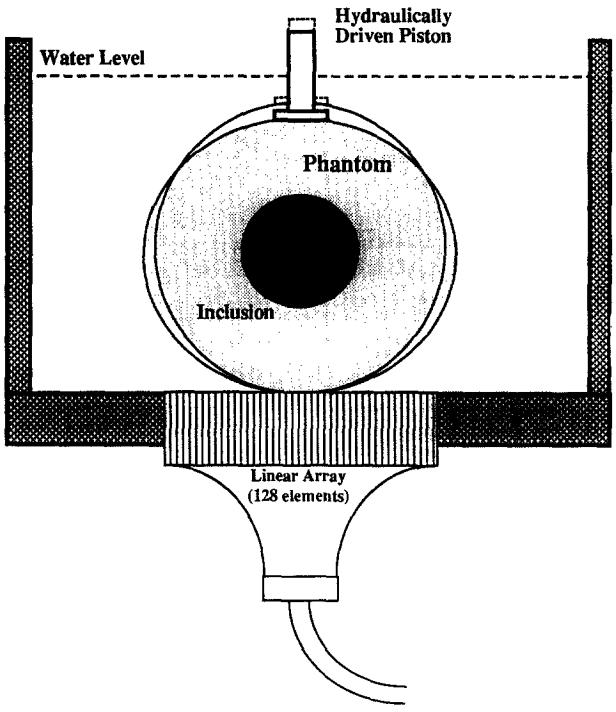

Fig. 13. Schematic of displacement and strain imaging geometry. A cylindrical phantom 88-mm diameter and 150-mm length was used, where a single piston vertically deformed the phantom as shown. The bottom of the phantom contacted a 128 element transducer array, which imaged the phantom cross section at the central plane. (Reprinted with permission from: O'Donnell M et al. Internal displacement and strain imaging using ultrasonic speckle tracking. *IEEE Transactions on Ultrasonics, Ferroelectrics, and Frequency Control* 1994;41(3):318, Figure 4. ©1994 IEEE.)

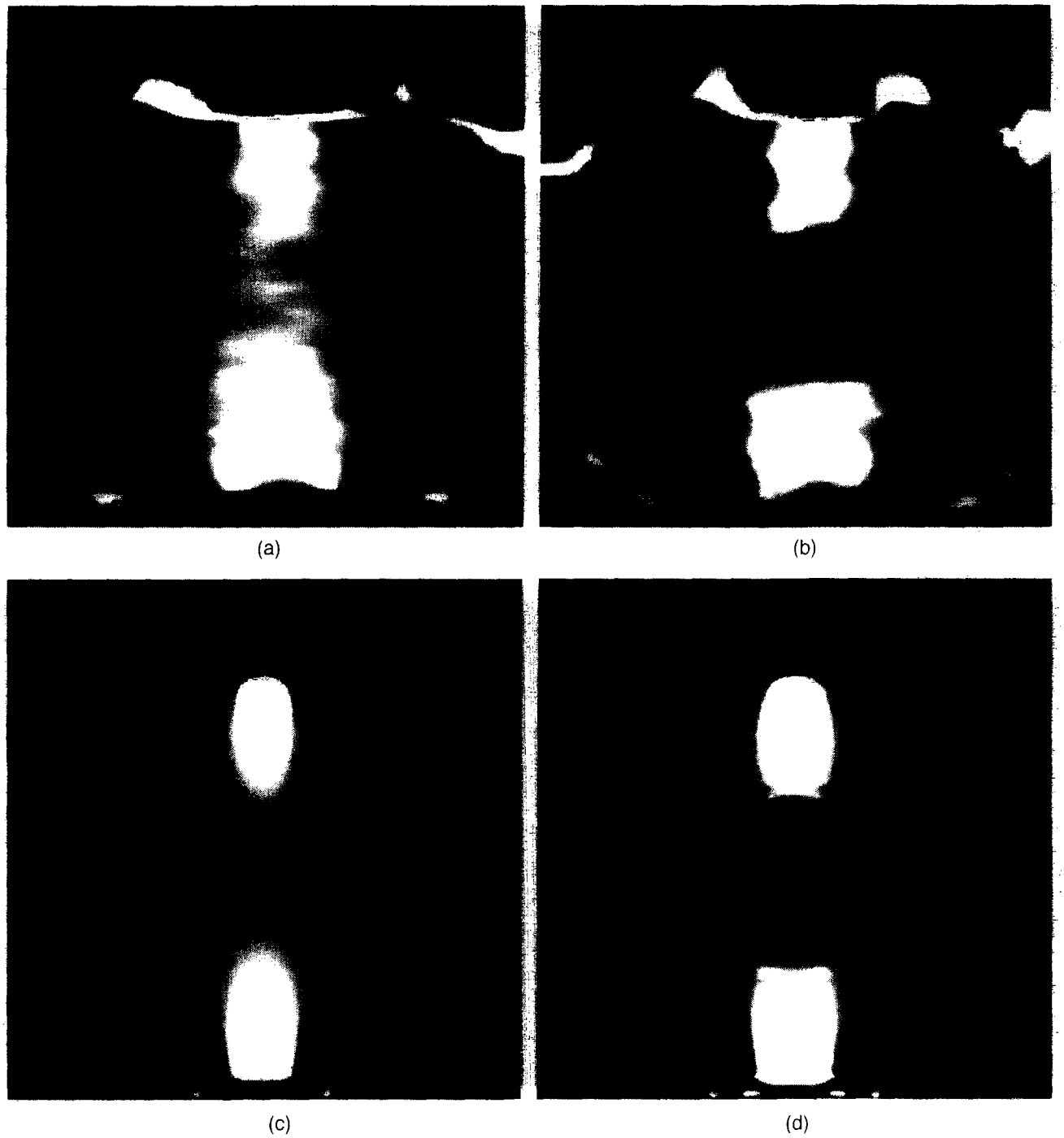

Fig. 14. Measured images of the vertical E_{22} component of the strain tensor for the (a) homogeneous and (b) inhomogeneous phantoms are compared with model predictions for the same (c) homogeneous and (d) inhomogeneous phantoms. Note that all images are displayed over the same absolute dynamic range. (Reprinted with permission from: Skovoroda AR, et al. Theoretical analysis and verification of ultrasound displacement and strain imaging. *IEEE Transactions on Ultrasonics, Ferroelectrics and Frequency Control* 1994;41(3):310, Figure 8. ©1994 IEEE.)

Multiple step compression strain sonoelastography

A research group at the University of Michigan, Ann Arbor, headed by O'Donnell has developed an approach to compression strain sonoelastography. They presented a two-dimensional analytical model for the forward problem (O'Donnell et al. 1994; Skovoroda et al. 1994): given the Young's modulus as a function of position, predict the strain inside

tissue given specific forces and boundary conditions. The governing equations for the static deformation of an isotropic, viscoelastic and incompressible medium were derived from Newton's second law, incompressibility, and from stress–strain relationships. The simplified two-dimensional equations are as follows:

$$\frac{\partial p}{\partial x_1} + 2\frac{\partial}{\partial x_1} \times \left(\mu \frac{\partial u_1}{\partial x_1}\right) + \frac{\partial}{\partial x_2}\left[\mu\left(\frac{\partial u_1}{\partial x_2} + \frac{\partial u_2}{\partial x_1}\right)\right] = 0 \quad (9a)$$

$$\frac{\partial p}{\partial x_2} + 2\frac{\partial}{\partial x_2}\left(\mu \frac{\partial u_2}{\partial x_2}\right) + \frac{\partial}{\partial x_1} \times \left[\mu\left(\frac{\partial u_1}{\partial x_2} + \frac{\partial u_2}{\partial x_1}\right)\right] + f_2 = 0 \quad (9b)$$

$$\frac{\partial u_1}{\partial x_1} + \frac{\partial u_2}{\partial x_2} = 0 \quad (9c)$$

where u_1 and u_2 are displacements for each point along the x_1 and x_2 directions, respectively. Referring to Fig. 13, x_1 is along the horizontal direction and x_2 is along the vertical direction. μ is proportional to Young's modulus, p is static internal pressure and f_2 is the body force. This set of equations with boundary conditions cannot be solved analytically except in very few extreme situations, so a finite difference method was used to obtain the solution iteratively.

The experimental apparatus used to test the model is shown in Fig. 13. The technique used to detect the strain inside the medium after deformation is based on cross-correlation of ultrasound A-lines. O'Donnell's group (O'Donnell et al. 1994; Skovoroda et al. 1994) suggested using large deformation to maximize the signal-to-noise ratio of the displacement and strain estimation. However, large displacement (over 10 wavelengths of the carrier signal) results in significant internal strain, which changes the spatial distribution of the scatters within the area of an image, thus decorrelating the speckle patterns used for cross-correlation. Consequently, they used multiple small step deformations (each step was less than one wavelength) to result in a large total deformation. The total displacement was then calculated by accumulating the displacements between each small deformation. For signal processing, they used base-band (not RF) correlation to determine the displacement inside tissue after each small deformation. The time shift between the pre- and postdefor-

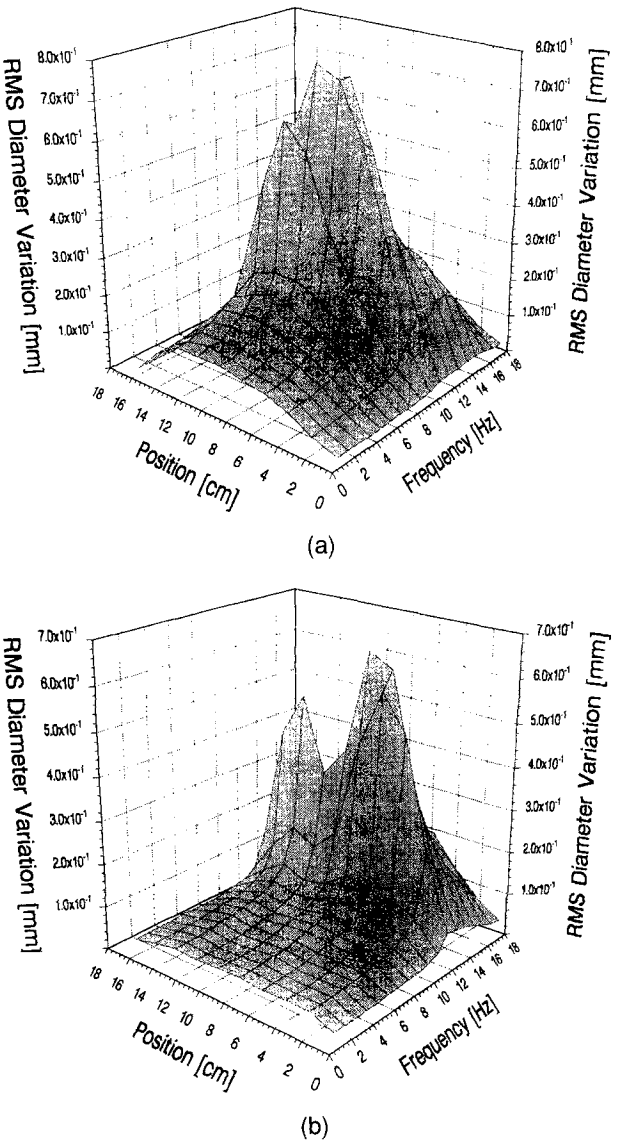

Fig. 15(a). Rigid wall model: diameter variation vs. position along the tube and frequency of vibration exciter for a latex tube of static diameter D_0 = 12.1 mm, length L = 20 cm, and P_t = 686 Pa. (Reprinted with permission from: Berrios CB, Pedersen CP. Ultrasonic measurement of forced diameter variations in an elastic tube. *Ultrasonic Imaging* 1994; 16:124–142, Figure 10.). (b). Rigid wall model: diameter variation vs. position along the tube and frequency of vibration exciter for a latex tube of static diameter D_0 = 12.1 mm, length L = 20 cm, and P_t = 686 Pa. An increase in stiffness was introduced over a region of the tube, extending from x_1 = 9 cm to x_2 = 11.5 cm. (Reprinted with permission from: Berrios CB, Pedersen CP. Ultrasonic measurement of forced diameter variations in an elastic tube. *Ultrasonic Imaging* 1994; 16:124–142, Figure 11.)

mation signals can be estimated from the phase of their zero-lag correlation functions:

$$t_{BB} = \frac{\tan^{-1}\left[\frac{\mathrm{Im}(\tilde{C}(0))}{\mathrm{Re}(\tilde{C}(0))}\right]}{\omega_0} \quad (10)$$

where $\tilde{C}$ is the base-band correlation function. A limitation associated with phase processing is that aliasing occurs if the displacement exceeds a quarter of an ultrasound wavelength (*i.e.*, $\lambda/4$). To overcome this limitation, they evaluated the differential displacement between neighboring vertical pixels, and then integrated it starting at a known position. A low pass filtering prior to phase detection can help to obtain better results. The vertical strain is the spatial derivative of vertical displacement. In this case, differential displacement was already calculated, so the strain was easily obtained.

In Fig. 14, examples of the strain images Skovoroda et al. (1994) obtained for homogeneous and inhomogeneous phantoms are compared with the images of corresponding theoretical predictions derived from the model.

O'Donnell's group (O'Donnell et al. 1994; Skovoroda et al. 1994) also posed the inverse problem: to construct a Young's modulus image given strain images. As the technique uses finite difference calculations, the solution may not converge if the initial guess is inadequate. Some preliminary results on reconstructing elasticity images were given in their other publications (O'Donnell et al. 1993). Kallel et al. (1994) have suggested other reconstruction schemes. Base-band correlation between A-line pairs is employed to estimate displacement. Multiple steps of compression are used to reduce the speckle decorrelation effect. The basic model is two-dimensional. The data process is done offline. Phantom and some *in vitro* results are presented.

Inherent strain elastography

Bertrand and colleagues (1989) proposed a biomechanical strain gauge using B-scan information and an optical flow algorithm. They modelled tissue deformation on consecutive B-scan images as linear transformations (Bertrand et al. 1989; Kallel and Bertrand 1993; Meunier et al. 1989). These linear transformations can be decomposed into rotation matrices and biaxial translation matrices. By calculating the eigenvalues of these matrices in a small region, the strain in that small region can be obtained. They suggested

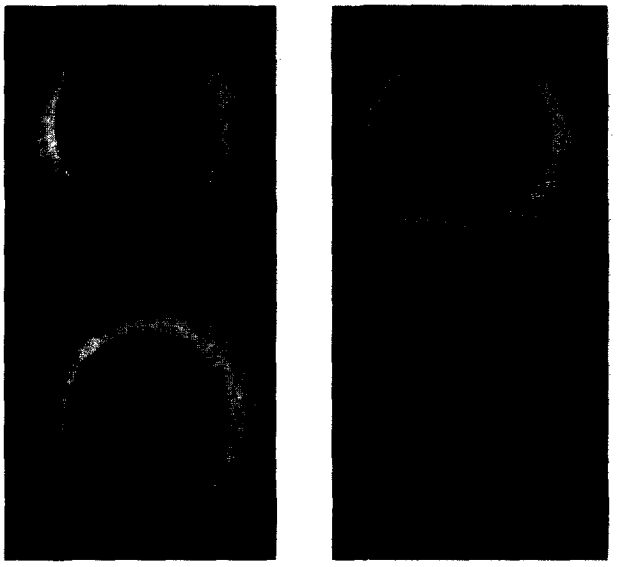

Fig. 16. (a) Cross-sectional images of gelatin vessel phantoms at mean pressure of 100 mmHg: (top) one-component soft phantom, (bottom) two-component phantom. The position of the transducer in the vessel lumen is indicated by the small cross and the scan rotation direction is clockwise from marked Oo reference. (b) Corresponding gray scale displacement maps for the pressure increment from 100 to 120 mmHg. (Reprinted with permission from: Ryan LK, Lockwood GR, Bloomfield TS, Foster FS. Speckle tracking in high frequency ultrasound image with application to intravascular image. *Proc IEEE Ultrasonics Symp* 1993; 889–892, Figure 5.)

further applications of this technique to elasticity estimates of skeletal muscle, and also described an important artifact in apparent speckle motion during tissue rotation (Kallel et al. 1994).

Tissue motion with speckle tracking

Trahey and his colleagues (Bohs and Trahey 1991) have developed a two-dimensional speckle tracking technique to measure blood flow and motion in soft tissue. The speckle tracking system employs a sum of absolute difference (SAD) method to estimate tissue motion in two dimensions. The echo data are first obtained for a two-dimensional kernel region of size $m \times n$: $k(i, j)$. At a later time, data for a search region including and surrounding the kernel region are acquired: $s(i, j)$. The following equation is evaluated for each α and β until a minimum of $\epsilon(\alpha, \beta)$ occurs:

$$\varepsilon(\alpha, \beta) = \sum_{i=1}^{m} \sum_{j=1}^{n} |k(i, j) - s(i + \alpha, j + \beta)|. \quad (11)$$

Then, (α, β) is the movement of the kernel region be-

tween the time of the first and the second data acquisitions.

In an application to vibration amplitude sonoelastography, Walker et al. (1993) measured tissue motion excited by externally applied vibration. Their system utilizes three major components: an electromechanical vibrator to excite tissue motion, an ultrasound scanner that can output either RF or detected echo data and a speckle tracking system for motion estimation. A synchronization is made among the three components so that phase information is preserved. The two-dimensional displacement information is displayed in real-time as two-dimensional map of colors.

Other quantitative characterization techniques

In this section, we summarize other recent developments related to elastography or measurements of local elastic properties and tissue motion.

Characterization of elastic vessels. Berrios and Pedersen (1994) studied an elasticity parameter of an elastic tube, the apparent compliance. They used ultrasound pulse–echo to measure the diameter variation of the tube in response to externally applied time-varying pressure functions. In the experiments, they first used pulse–echo to obtain signals from the back and front walls of a latex tube under ambient pressure. These signals were called the reference signals. A sinusoidally varying pressure was then applied to the tube, and the echoed signals were cross-correlated with the reference signals. The diameter change of the tube was easily estimated by using these cross-correlations, given the knowledge of the ultrasound propagation speed.

Berrios and Pedersen (1994) made measurements along a 20-cm-long tube under different forcing frequencies (Fig. 15). Some interesting observations were: (1) the tube had apparent resonant frequencies and (2) the diameter variation decreased at the location of increased stiffness. The localized increase in tube stiffness may serve as a simple model for vessel pathology such as arteriosclerosis.

A research group in Toronto headed by Foster (Ryan et al. 1992, 1993) also studied vessel wall displacement under applied pressure. In their experiments, they placed a radially oriented 42-MHz single element transducer inside the tube under study. Complete cross-sectional scans were acquired by rotating the transducer outer housing through 360°. A correlation search technique was employed to assess the tube wall displacement. Images from this experiment are shown in Fig. 16. The investigators claimed a system detection sensitivity of 10 μm axially and 20 μm laterally by the ultrasound beam direction. The data processing, including correlation searching, was done offline.

Fetal movements. There have been further developments in the study of fetal lung movement. Fetal movement reflects fetal condition and neural condition, and evaluation of this movement may be valuable in the management of high-risk pregnancy. Shinozuka and coworkers (Shinozuka and Yamakoshi 1993; Shinozuka et al. 1994) used a multichannel pulsed Doppler system to monitor fetal movements. Each channel processes signals echoed from one point inside the fetus along the ultrasound beam direction, and the points are separated by 1.5 cm. The displacements are estimated by an arc-tangent method, that is, by calculating the phase shift from the quadrature components of the signal by:

$$\Delta\chi = \frac{c}{2\omega}\left[\tan^{-1}\left(\frac{Q(t)}{I(t)}\right) \pm n\pi\right] \qquad (12)$$

where c is the speed of ultrasound, ω is the frequency and $Q(t)$ and $I(t)$ are the quadrature and in-phase components of the signal. $n\pi$ is used to offset the displacement from zero-crossing points of $I(t)$. These investigators also classified the characteristics of three different movements: fetal breath movement (FBM), fetal gross movement (FGM) and fetal heart movement (FHM), based on the different frequency ranges and amplitudes of the movements. Then they used the maximum entropy method to separate the different movements. Some *in vivo* movement tracking records are shown in Fig. 17.

Tissue motion with MRI. Zerhouni et al. (1988) proposed a tagging MRI technique to assess myocardial motion. A key procedure in this technique is application of a selective RF pulse to sections of tissue before imaging. This is done in the presence of a linear magnetic gradient field, so the magnetization of protons in those sections is perturbed. Before the full recovery of magnetization in the areas, an MR image of the tissue is obtained in a plane orthogonal to the tagged planes. Due to the different degrees of saturation, the signals will be different between the tagged and untagged regions. The motion occurring during the tagging and imaging interval will be reflected by displacement and distortion of the tagged regions. An experimental result demonstrating motion is shown in Fig. 18. Some studies using similar a technique have been reported by Axel and Dougherty (1989a, 1989b). Very recent work from the Mayo Clinic reports a direct

MRI visualization of shear waves (Muthupilli et al., 1995).

Measurement of intraocular pressure. Richards and collaborators (Alam et al. 1992, 1994) have applied vibration amplitude sonoelastography to the eye with a goal of detecting intraocular pressure (IOP). The basic postulate is that the sclera is a tough, nonlinear elastic shell with spherical geometry. Natural resonances of the eye can be excited at different frequencies and detected by Doppler ultrasound. As IOP increases, the sclera stiffens appreciably, shifting the resonance frequencies of the eye. Preliminary *in vitro* and *in vivo* results have supported the basic concept; however, the accuracy of the technique in clinical use remains to be studied.

CONCLUSION

Tissue elasticity has always been an important concept in the fields of medicine and biology. The combination of this concept with modern imaging systems has generated elastography techniques. Although these techniques still require further development to become reliable modalities, work to date has established their potential for providing useful clinical diagnostic information that cannot be obtained by traditional medical imaging.

A number of issues remain unanswered and require further study before elastography is optimized and can be introduced into clinical use. Some of these are:

1. *Elasticity data.* There is a great need for reliable measurements of the elastic properties of tissue in the normal state and in different pathological conditions. These data are critical to the generation, evaluation and interpretation of different elastography strategies.
2. *Source excitation.* In both static measurements and dynamic (vibration) sonoelastography, there is a need to optimize the source of mechanical excitation, in spatial and temporal (frequency) terms. The goal is to optimize the resulting image and permit the best possible interpretation of the underlying pathology.
3. *Tissue models.* The early models for elastography

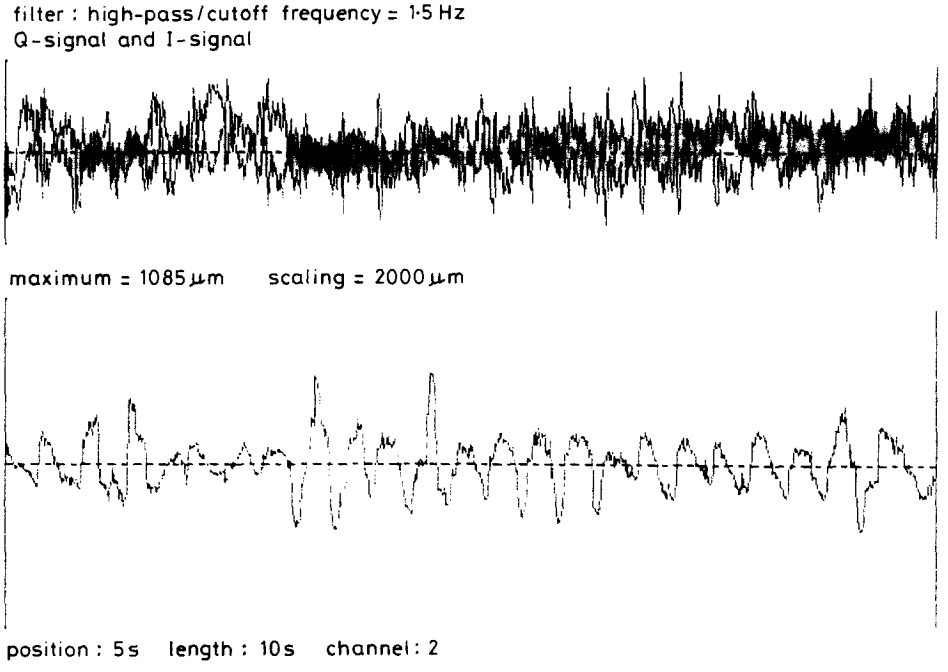

Fig. 17. Displacements derived from fetal heart movements extracted by digital signal filtering. From the fetal tissue displacement measurement, the components of FHM were extracted. In this case, the sampling point was at the fetal abdomen, not at the fetal heart. The vibration of fetal tissue by the heart movement was extracted. The upper row shows the original Q and I signals. The lower row shows the displacements derived from FHM processed by 1·5 HZ digital high-pass filtering. Sinusoidal movements with an amplitude of 1 mm are extracted. The displacement of 23 cycles in 10 s means that the fetal heart rate is 138 beats min^{-1} (case at 37 weeks' gestation: 10 s chronogram). (Reprinted with permission from: Shinozuka N, Yamakoshi Y. Measurement of fetal movements using multichannel ultrasound pulsed Doppler: Autorecognition of fetal movements by maximum entropy method. *Medical & Biological Engineering and Computing* 1993;31(Suppl.):S59–S66, Figure 4.)

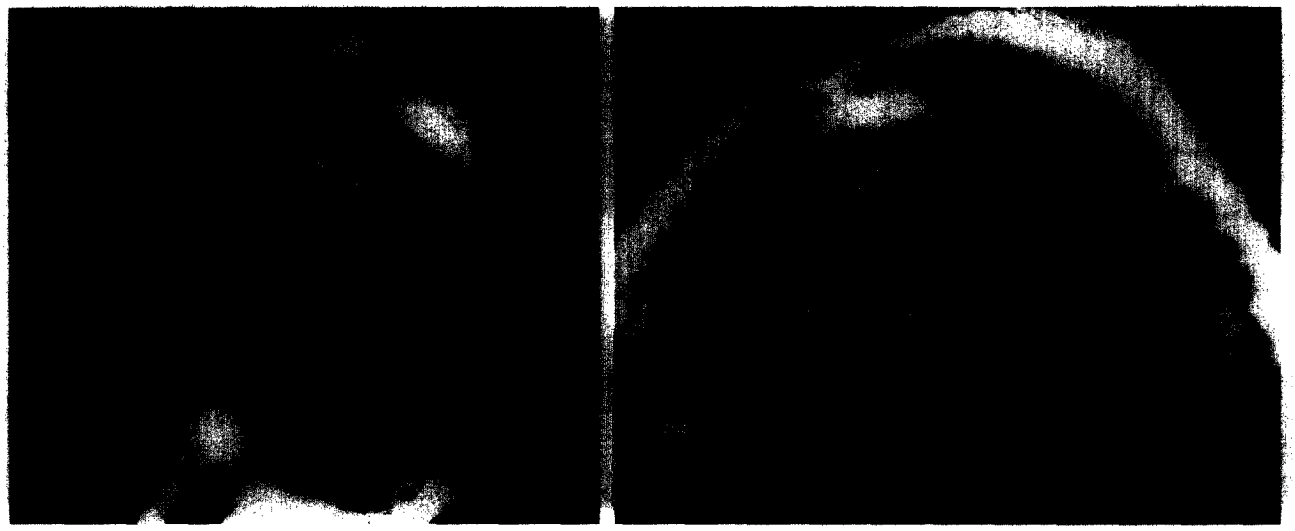

(a) (b)

Fig. 18. (a) Two triple-frequency, selective, 180° RF pulses were generated 12 msec apart at mid-diastole in a plane perpendicular to the long axis of the heart. This separately tagged the base and apex with three 0.35-cm thick parallel planes separated by 0.35 cm of nontagged tissue. The heart was then imaged 250 msec later at about mid-systole in the long axis. Note the motion of the tagged regions relative to their original location, indicated by the set of dark lines in the thoracic wall structures (arrowheads). Group of tag lines at base (solid arrows) has moved toward the apex by 15 mm for the most basal line and by 10 mm for the most apical line. Degree of contraction of the muscle is recorded by decreased separation between tag lines at the base compared with that between the apical tags. Group of lines at apex (open arrow) demonstrates that most apical region of left ventricle has moved very little. This experiment demonstrates ability of the technique to identify and quantify the regional (base-vs-apex) motion patterns as well as intrinsic changes due to contraction (with tag-separation measurements). (b) Two orthogonal sets of three-lobed RF pulses imposed at diastole have imprinted a gridlike pattern on the myocardium. Imaging in the short axis of the left ventricle at early systole demonstrates intervening deformation and reorientation of the tag lines relative to their diastolic position, indicated by the chest wall tags. Tags in the subcutaneous and epicardial fat are not demonstrated, because of the shorter T1 relaxation time of fat. (Reprinted with permission from: Zerhouni EA. Human heart: Tagging with MR imaging—A method for noninvasive assessment of myocardial motion. *Radiology* 1988;169(1):61, Figures 4 and 5.)

assume simple linear isotropic elastic behavior. The appropriateness and limitations of these simple models require further examination in view of the widespread recognition of the complicated nature of tissues, including nonlinear behavior, hysteresis effects and complex viscoelastic temporal response.

4. *Boundary conditions.* The nature of organ–organ or tissue–tissue boundary conditions is not well understood, yet these boundaries are important in a wide range of compression and vibration sonoelastography applications. Do fat globules slip out-of-plane under different loading conditions? How well can displacements (or shear waves) be transmitted across the liver–kidney boundary? These types of questions will require careful experimental and theoretical treatment.

The early applications of sonoelastography have been quite promising, and the results clearly indicate that new information, previously unavailable in conventional imaging modalities, can now be obtained.

Acknowledgements—Support from NSF/NYS Center for Electronic Imaging Systems is gratefully acknowledged. We appreciate the advice of S. K. Alam and D. Rubens in preparing the manuscript.

REFERENCES

Adler R, Rubin JM, Bland P, Carson P. Characterization of transmitted motion in fetal lung: Quantitative analysis. Med Phys 1989;16:333–337.

Adler RS, Barbosa DC, Cosgrove DO, Nassiri DK, Bamber JC, Hill CR. Quantitative tissue motion analysis of digitized M-mode images: Gestational differences of fetal lung. Ultrasound Med Biol 1990;16:561–569.

Alam SK, Richards DW, Parker KJ. Detection of intraocular pressure change in a human eye model using sonoelastic Doppler ultrasound. Proceedings IEEE Ultrasonics Symposium, 1992: 1057–1060.

Alam SK, Richards DW, Parker KJ. Detection of intraocular pressure change in the eye using sonoelastic Doppler ultrasound. Ultrasound Med Biol 1994;20:751–758.

Axel L, Dougherty L. Heart wall motion: Improved method of spatial

modulation of magnetization for MR imaging. Radiology 1989a;172:349–350.
Axel L, Dougherty L. MR imaging of motion with spatial modulation of magnetization. Radiology 1989b;171:841–845.
Bertrand M, Meunier J, Doucet M, Ferland G. Ultrasonic biomechanical strain gauge based on speckle tracking. Proceedings IEEE Ultrasonics Symposium, 1989:859–863.
Berrios JC, Pedersen PC. Ultrasonic measurement of forced diameter variations in an elastic tube. Ultrason Imaging 1994;16:124–142.
Birnholz JC, Farrell EE. Fetal lung development: Compressibility as a measure of maturity. Radiology 1985;157:495–498.
Bohs LN, Trahey GE. A novel method for angle independent ultrasonic imaging of blood flow and tissue motion. IEEE Trans Biomed Eng 1991;BME-38:280–286.
Buchtal F, Kaiser E. The rheology of the cross striated muscle fibre with particular reference to isotonic conditions. Det K Dan Vidensk Selsk Copenhagen Dan Biol Med 1951;21:328.
Carstensen E, Schwan H. Acoustic properties of hemoglobin solutions. J Acoust Soc Am 1959;31:305–311.
Céspedes I, Ophir J. Reduction of image noise in elastography. Ultrason Imaging 1993;15:89–102.
Céspedes I, Ophir J, Ponnekanti H, Maklad N. Elastography: Elasticity imaging using ultrasound with application to muscle and breast *in vivo*. Ultrason Imaging 1993;15:73–88.
Cox M, Rogers PH. Automated noninvasive motion measurement of auditory organs in fish using ultrasound. J Vibrat Acoust Stress Reliabil Des 1987;109:55–59.
De Jong PGM, Arts T, Hoeks APG, Reneman RS. Determination of tissue motion velocity by correlation interpolation of pulsed ultrasonic echo signals. Ultrason Imaging 1990;12:84–98.
Dickinson RJ, Hill CR. Measurement of soft tissue motion using correlation between A-scans. Ultrasound Med Biol 1982;8:263–271.
Eisensher A, Schweg-Toffler E, Pelletier G, Jacquemard G. La palpation échographique rythmée-echosismographie. J Radiol 1983;64:255–261.
Fung YC. Biomechanics—cechanical properties of living tissues. New York: Springer-Verlag Inc., 1981.
Gao L, Alam SK, Lerner RM, Parker KJ. Sonoelasticity imaging: Theory and experimental verification. J Acoust Soc Am, 1995;97:3875–3886.
Holen J, Waag RC, Gramiak R. Representation of rapidly oscillating structures on the Doppler display. Ultrasound Med Biol 1985;11:267–272.
Huang SR, Lerner RM, Parker KJ. On estimating the amplitude of harmonic vibration from the Doppler spectrum of reflected signals. J Acoust Soc Am 1990;88:310–317.
Huang SR, Lerner RM, Parker KJ. Time domain Doppler estimators of the amplitude of vibrating targets. J Acoust Soc Am 1992;91:965–974.
Jarzynski J, Lee D, Vignola J, Berthelot H, Pierce AD. Fiber optics Doppler systems for remote sensing of fluid flow. In: Ocean optics IX, Proceedings of SPIE Conference on Optics, Electro-Optics, and Sensors, Apr. 4–6, 1988, volume 925. Bellingham, WA: SPIE—The International Society for Optical Engineering, 1988:250–254.
Kallel F, Bertrand M. A note on strain estimation using correlation techniques. Proceedings IEEE Ultrasonics Symposium, 1993:883–887.
Kallel F, Bertrand M, Meunier J. Speckle motion artifact under tissue rotation. IEEE Trans Ultrason Ferroelectr Freq Control 1994;41:105–122.
Krouskop TA, Dougherty DR, Levinson SF. A pulsed Doppler ultrasonic system for making noninvasive measurements of the mechanical properties of soft tissues. J Rehabil Res Biol 1987;14:1–8.
Laurence NB, Trahey GE. A novel method for angle independent ultrasonic imaging of blood flow and tissue motion. IEEE Trans Biomed Eng 1991;38:280–286.
Lee F, Bronson JP, Lerner RM, Parker KJ, Huang SR, Roach DJ. Sonoelasticity imaging: Results in *in vitro* tissue specimens. Radiology 1991;181:237–239.
Lerner RM, Parker KJ. Sonoelasticity images derived from ultrasound signals in mechanically vibrated targets. In: Tjissen J, ed. Proceedings of the Seventh European Communities Workshop. Nijmegen, The Netherlands, 1987.
Lerner RM, Parker KJ, Holen J, Gramiak R, Waag RC. Sono-elasticity: Medical elasticity images derived from ultrasound signals in mechanically vibrated targets. Acoust Imaging 1988;16:317–327.
Lerner RM, Huang SR, Parker KJ. Sonoelasticity images derived from ultrasound signals in mechanically vibrated tissues. Ultrasound Med Biol 1990;16:231–239.
Levinson SF. Ultrasound propagation in anisotropic soft tissues: The application of linear elastic theory. J Biomech 1987;20:251–260.
Levinson SF, Shinagawa M, Sato T. Sonoelastic determination of human skeletal muscle elasticity. J Biomech 1995;28:1145–54.
Meunier J, Bertrand M, Faouzi K. A model of speckle motion artifacts occurring under tissue linear transformation. Ultrason Imaging 1989;11:133.
Muthupilli R, Lomas D, Rossman P, Greenleaf J, Manduca A, Ehman R. MR elastography by direct visualization of propagating acoustic strain waves. Science 1995;269:1854–1856.
O'Donnell M, Emelianov SY, Skovoroda AR, Lubinski MA, Weitzel WF, Wiggins RC. Quantitative elasticity imaging. Proceedings IEEE Ultrasonics Symposium, 1993:893–903.
O'Donnell M, Skovoroda AR, Shapo BM, Emelianov SY. Internal displacement and strain imaging using ultrasonic speckle tracking. IEEE Trans Ultrason Ferroelectr Freq Control 1994;41:314–325.
Oestreicher HL. Field and impedance of an oscillating sphere in a viscoelastic medium with an application to biophysics. J Acoust Soc Am 1951;23:707–714.
Ophir J, Céspedes I, Ponnekanti H, Yazdi Y, Li X. Elastography: A quantitative method for imaging the elasticity of biological tissues. Ultrason Imaging 1991;13:111–134.
Parker KJ, Huang SR, Lerner RM, Lee F Jr, Rubens D, Roach D. Elastic and ultrasonic properties of the prostate. Proceedings IEEE Ultrasonics Symposium, 1993:1035–1037.
Parker KJ, Huang SR, Musulin RA. Tissue response to mechanical vibrations for sonoelasticity imaging. Ultrasound Med Biol 1990;16:241–246.
Parker KJ, Lerner RM. Sonoelasticity of organs: Shear waves ring a bell. J Ultrasound Med 1992;11:387–392.
Pauly H, Schwan H. Mechanism of absorption of ultrasound in liver tissues. J Acoust Soc Am 1971;50:692–699.
Ponnekanti H, Ophir J, Céspedes I. Axial stress distributions between coaxial compressors in elastography: An analytical model. Ultrasound Med Biol 1992;18:667–673.
Rubens DJ, Hadley MA, Alam SK, Gao L, Mayer RD, Parker KJ. Sonoelastic imaging of prostate cancer: *In vitro* results. Radiology, 1995;195:379–383.
Ryan LK, Lockwood GR, Bloomfield TS, Foster FS. Speckle tracking in high frequency ultrasound images with application to intravascular imaging. Proceedings IEEE Ultrasonics Symposium, 1993:889–892.
Ryan LK, Lockwood GR, Starkoski BG, Holdsworth DW, Rickey DW, Drangova M, Fenster A, Foster FS. A high frequency intravascular imaging system for investigation of vessel wall properties. Proceedings IEEE Ultrasonics Symposium, 1992:1101–1105.
Saada AS. Elasticity, theory and applications. New York: Pergamon Press, 1974:395–428.
Sato T, Fukusima A, Ichida N, Ishikawa H, Miwa H, Igarashi Y, Shimura T, Murakami K. Nonlinear parameter tomography system using counterpropagating probe and pump waves. Ultrason Imaging 1985;7:49–59.
Shinozuka N, Yamakoshi Y. Measurement of fetal movements using multichannel ultrasound pulsed Doppler: Autorecognition of fetal movements by maximum entropy method. Med Biol Eng Comput 1993;31:S59–S66.
Shinozuka N, Yamakoshi Y, Taketani Y. New method for tracking

fetal breathing movements using real-time pulsed Doppler ultrasonographic displacement measurement. J Ultrasound Med 1994;13:19–25.

Skovoroda AR, Emelianov SY, Lubinski MA, Sarvazyan AP, O'Donnell M. Theoretical analysis and verification of ultrasound displacement and strain imaging. IEEE Trans Ultrason Ferroelectr Freq Control 1994;41:302–313.

Taber LA. Large deformation mechanics of the enucleated eyeball. J Biomech Eng 1984;106:229–234.

Taylor KJ. Absolute measurement of acoustic particle velocity. J Acoust Soc Am 1976;59:691–694.

Taylor KJ. Absolute calibration of microphones by a laser-Doppler technique. J Acoust Soc Am 1981;70:939–945.

Tristam M, Barbosa DC, Cosgrove DO, Nassiri DK, Bamber JC, Hill CR. Ultrasonic study of *in vivo* kinetic characteristics of human tissues. Ultrasound Med Biol 1986;12:927–937.

Tristam M, Barbosa DC, Cosgrove DO, Nassiri DK, Bamber JC, Hill CR. Application of Fourier analysis to clinical study of patterns of tissue movement. Ultrasound Med Biol 1988;14:695–707.

Truong XT. Extensional wave-propagation characteristics in striated muscle. J Acoust Soc Am 1971;51:1352–1356.

Viidik A. Biomechanics and functional adaptation of tendons and joint ligaments. In: Evans FG, ed. Studies on the anatomy and function of bone and joints. New York: Springer-Verlag, 1966:17–39.

Von Gierke HE, Oestreicher HL, Franke EK, Parrack HO, Von Wittern WW. Physics of vibrations in living tissues. J Appl Physiol 1952;4:886–900.

Walker WF, Friemel BH, Laurence NB, Trahey GE. Real-time imaging of tissue vibration using a two-dimensional speckle tracking system. Proceedings IEEE Ultrasonics Symposium, 1993:873–877.

Wilson LS, Robinson DE. Ultrasonic measurement of small displacements and deformations of tissue. Ultrason Imaging 1982;4:71–82.

Yamakoshi Y, Sato J, Sato T. Ultrasonic imaging of internal vibration of soft tissue under forced vibration. IEEE Trans Ultrason Ferroelectr Freq Control 1990;37:45–53.

Zerhouni EA, Parish DM, Rogers WJ, Yang A, Shapiro EP. Human heart: Tagging with MR imaging—A method for noninvasive assessment of myocardial motion. Radiology 1988;169:59–63.